CELL BIOLOGY

Circadian regulation of protein cargo in extracellular vesicles

Ching-Yan Chloé Yeung[1,2]*, Frank Dondelinger[3], Erwin M. Schoof[4], Birgitte Georg[5], Yinhui Lu[6], Zhiyong Zheng[7], Jingdong Zhang[7], Jens Hannibal[5,8], Jan Fahrenkrug[5], Michael Kjaer[1,2]

The circadian clock controls many aspects of physiology, but it remains undescribed whether extracellular vesicles (EVs), including exosomes, involved in cell-cell communications between tissues are regulated in a circadian pattern. We demonstrate a 24-hour rhythmic abundance of individual proteins in small EVs using liquid chromatography–mass spectrometry in circadian-synchronized tendon fibroblasts. Furthermore, the release of small EVs enriched in RNA binding proteins was temporally separated from those enriched in cytoskeletal and matrix proteins, which peaked during the end of the light phase. Last, we targeted the protein sorting mechanism in the exosome biogenesis pathway and established (by knockdown of circadian-regulated flotillin-1) that matrix metalloproteinase 14 abundance in tendon fibroblast small EVs is under flotillin-1 regulation. In conclusion, we have identified proteomic time signatures for small EVs released by tendon fibroblasts, which supports the view that the circadian clock regulates protein cargo in EVs involved in cell-cell cross-talk.

INTRODUCTION

In mammals, the circadian clock is responsible for producing daily rhythms in crucial homeostatic processes in anticipation of environmental changes during 24 hours, including regulating body temperature, sleep activity, feeding, and metabolism. Almost all peripheral tissues have a self-sustaining molecular oscillator that generates a 24-hour periodicity of tissue-specific clock-controlled outputs (*1*). Misalignment of peripheral circadian rhythms caused by jet lag, shift work, sleep disruptions, and aging is linked to increased morbidity and mortality (*2*). Synchronization of peripheral tissue circadian rhythms is mediated through a combination of non–light entrainment factors or "zeitgebers," e.g., feeding time or scheduled exercise, and stabilized by endogenous signals from the central clock (*1*, *2*). However, mechanisms of cell-cell and intertissue peripheral circadian clock entrainment have not yet been investigated. Understanding these mechanisms will explain how the circadian rhythms of different tissues in the body are coordinated.

The primary molecular oscillator responsible for generating a 24-hour rhythm is a transcription-translation feedback loop consisting of the following transcription factors: brain and muscle aryl hydrocarbon receptor nuclear translocator-like 1 (BMAL1) and circadian locomotor output cycles kaput (CLOCK) that drives the expression of clock-controlled genes, including period (PER) and cryptochrome (CRY). When cells are released from tissues and placed in tissue culture, the individual oscillators become asynchronous but can be easily resynchronized, for example, by administering glucocorticoids (*3*). Synchronizing cell cultures has enabled discoveries of how the circadian clock temporally coordinates various aspects of cell biology, for examples, actin dynamics (*4*), endocytosis (*5*), the secretory pathway (*6*), and, more recently, the secretion of collagen by mouse tendon fibroblasts (*7*), protein folding and endoplasmic reticulum stress (*8*, *9*), and autophagy (*10*, *11*). Whether the circadian clock also regulates exosome biogenesis, which produces 50- to 150-nm vesicles that mediate cell-cell communication within and between tissues, has not yet been studied.

Exosomes are synthesized, and their protein cargo is loaded in the endosomal pathway; their mode of communication includes the transfer of functional cargo, including proteins and RNA materials, into recipient cells (*12*, *13*). The circadian clock controls nearly 50% of protein-coding genes in mammalian tissues (*14*), and thus, we hypothesized that the proteome of extracellular vesicles (EVs) released by cells during 24 hours is time dependent.

One family of proteins that sorts proteins in the endosomal pathway is the flotillins (flotillin-1 and flotillin-2, encoded by *Flot1* and *Flot2*, respectively), which are lipid raft–associated proteins that localize to endosomes, lysosomes, and exosomes (*15*). Flotillins interact with a dileucine motif on the cargo protein to regulate their levels in specific membrane compartments (*16*). The expression of *Flot1* is circadian in a number of mouse tissues, including kidney, liver, lung, and tendon (*14*, *17*), suggesting a mechanism by which the circadian clock temporally regulates the protein content of EVs, including exosomes, and other endosomal compartments.

Tendon fibroblasts maintain their high synthetic activity and endogenous circadian rhythm in culture (*7*, *17*), which make them relevant to use for studying circadian clock–regulated cellular processes in vitro. An important membrane-localized protein necessary for tendons is matrix metalloproteinase 14 (MMP14 or MT1-MMP). MMP14 plays a critical role in the assembly of collagen-rich extracellular matrix (ECM) during development both in tendon and in many other tissues (*18*, *19*). This transmembrane protein contains a dileucine motif LLY573 in its cytoplasmic domain (*20*, *21*) and retains catalytic activity when localized to exosomes (*22*–*24*). On the basis of these data, we further hypothesized that MMP14 is also localized to tendon fibroblast EVs and that its levels in EVs can be regulated by flotillin-1.

[1]Institute of Sports Medicine Copenhagen, Department of Orthopedic Surgery, Copenhagen University Hospital–Bispebjerg and Frederiksberg, Copenhagen, Denmark. [2]Center for Healthy Aging, Department of Clinical Medicine, University of Copenhagen, Copenhagen, Denmark. [3]Centre for Health Informatics, Computation and Statistics, Lancaster University, Lancaster, UK. [4]Proteomics Core, Technical University of Denmark, Kongens Lyngby, Denmark. [5]Department of Clinical Biochemistry, Bispebjerg and Frederiksberg Hospital, Copenhagen, Denmark. [6]Wellcome Trust Centre for Cell-Matrix Research, Faculty of Biology, Medicine and Health, University of Manchester, Manchester, UK. [7]Department of Chemistry, Technical University of Denmark, Kongens Lyngby, Denmark. [8]Institute of Clinical Medicine, University of Copenhagen, Denmark.
*Corresponding author. Email: chloe.yeung@gmail.com

Here, we studied the role of the circadian clock in regulating protein cargo in small EVs. We used a proteomics approach to characterize the proteome profiles of a small EV time series isolated from synchronized tendon fibroblasts and explored the functional enrichment of these rhythmic EV proteins. Furthermore, we modulated endosomal protein sorting by targeting flotillin-1 and examined the effects on MMP14 localization.

RESULTS

Primary fibroblast cultures produce small EVs and maintain circadian rhythms

Small EVs isolated from primary cultures of tendon fibroblasts derived from *PER2::LUC* circadian reporter mice were analyzed by Western blotting and transmission electron microscopy (TEM). Western blot analysis comparing the purified small EV extract with total cell lysate confirmed that the EV fraction was positive for flotillin-1 and CD9 (a tetraspanin enriched in exosomes) as well as for other transmembrane proteins including integrins (α_2, α_5, and β_1) and MMP14, but enrichment for markers of several other membrane compartments, including intralumenal vesicles (caveolin-1), endoplasmic reticulum [heat shock protein 47 (HSP47)], and nucleus (RNA polymerase II and histone 3), was not detectable (Fig. 1A). TEM analysis of the EV fraction revealed vesicles with electron-dense membranes between 30 and 50 nm in size with a median diameter of 37.7 ± 13.8 nm (SD) (Fig. 1, B and C). TEM also confirmed that fibroblasts in culture contained the essential organelles required for exosome biogenesis, including endocytic vesicles at the plasma membrane, internal vesicles, multivesicular body, and lysosomes (Fig. 1D).

After synchronization using dexamethasone, the fibroblasts produced a rhythmic PER2:Luciferase signal with a period of 25.1 ± 0.1 hours (SD) that was evident for up to ~6 days (Fig. 1E). Analysis of whole-cell lysate from synchronized cells by Western blotting showed rhythmic MMP14 protein levels during 24 hours (Fig. 1F). Furthermore, gelatin zymography of time series cell lysates also showed rhythmic gelatinase activity by MMP2 (Fig. 1G), establishing that synchronized fibroblasts produced circadian rhythms in protein levels and activity.

Proteomic analysis of time series EVs from synchronized fibroblasts

A time series EV isolation protocol was designed, and to control for any effects from serum withdrawal, a control time series was isolated from unsynchronized cells (Fig. 2, A to C). Samples from the first

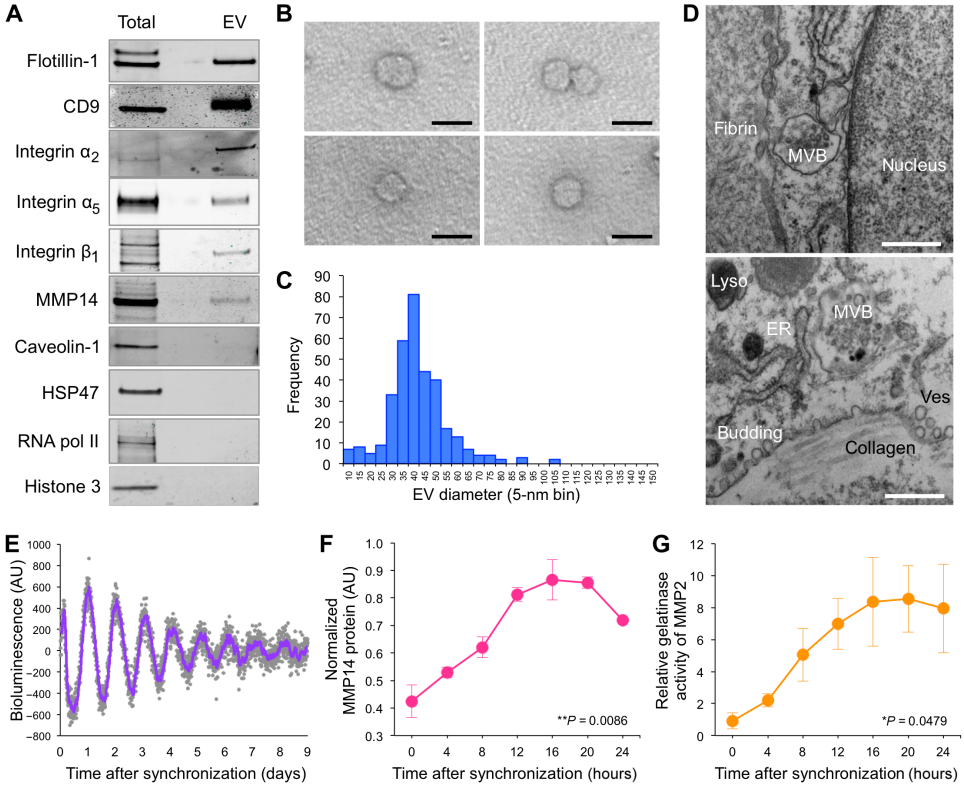

Fig. 1. Primary tendon cells in culture produce small EVs and maintain circadian rhythms. (**A**) Western blot analysis of whole-cell lysate and EVs purified from conditioned medium. Small EV extracts (EV) were positive for exosome markers, flotillin-1, CD9, and plasma membrane markers, including MMP14, and were negative for markers of other membrane compartments. (**B**) TEM images of purified small EVs showed membrane-bound vesicles. Scale bars, 50 nm. (**C**) Measurements from TEM images showed that the median diameter of small EVs released in media was 37.7 ± 13.8 nm (SD) (338 EVs measured from two independent conditioned medium purifications). (**D**) Representative TEM images showing features of the endosomal pathway [endocytic vesicles (Ves), multivesicular bodies (MVB), and lysosomes (Lyso)] and matrix assembly features [endoplasmic reticulum (ER) and collagen]. Scale bars, 500 nm. (**E**) Representative real-time bioluminescence recording of PER2::Luciferase activity in synchronized cells showed a circadian rhythm maintained for ~6 days with a mean period of 25.1 ± 0.1 hours (SD) ($n = 6$). (**F**) Quantification of MMP14 protein during 24 hours normalized to glyceraldehyde-3-phosphate dehydrogenase (GAPDH) loading control ($n = 3$ technical replicates except $n = 2$ for 24 hours; bars show SEMs; $^{**}P < 0.0086$, Kruskal-Wallis test). (**G**) Quantification of gelatinase activity of MMP2 (62-kDa band) relative to 0 hour ($n = 3$ from three independent assays; bars show SEMs; $^{*}P = 0.0479$ Kruskal-Wallis test). See data file S1 for original scans of Western blots and gels and uncropped TEM images. AU, arbitrary units.

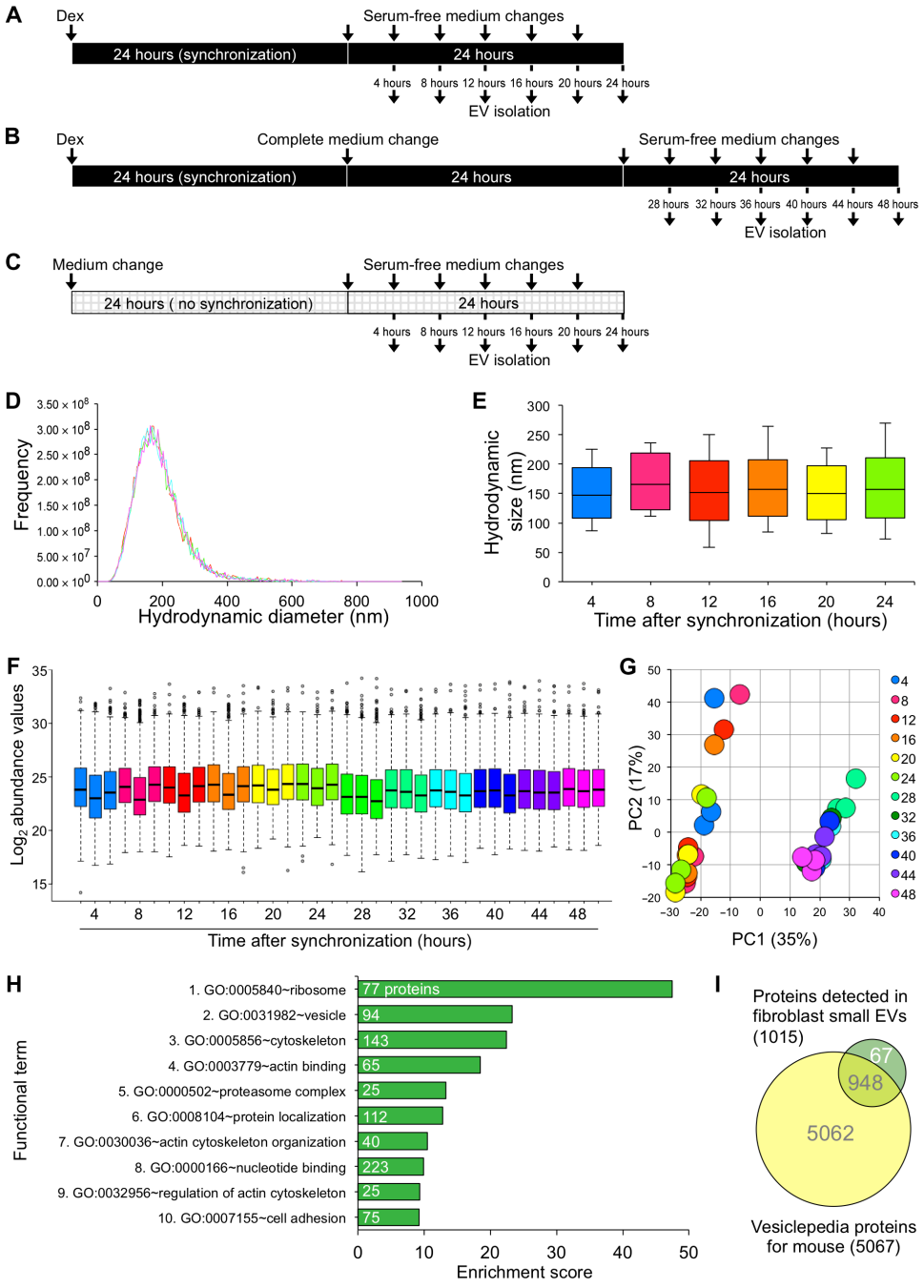

Fig. 2. Time series fibroblast small EV isolation for proteomics analysis. (**A**) Schematic diagrams the experimental setup for time series isolation of EVs from the first and (**B**) second 24 hours after synchronization with dexamethasone (Dex) and (**C**) from control (no synchronization) cells. Arrows above the bars indicate fresh medium changes. Arrows below the bars indicate media collected for sample isolations. (**D**) Representative NTA plot showing hydrodynamic diameters of small EVs released overnight into conditioned medium. The histograms are for each of the five technical replicates, each outlined in a different color, with a median diameter of 174.3 ± 77 nm (SD; $n = 5$ technical replicates from one experiment). (**E**) Box-and-whisker plot showing that the median hydrodynamic diameter of small EVs for 24 hours was unchanged (~170 nm). Data from one experiment are shown. (**F**) Box plot showing the distribution of protein abundances detected by LC-MS in triplicate samples of small EVs isolated during 48 hours after synchronization. (**G**) Principal components analysis (PCA) showing the first two principal components of variances between the 48-hour time series samples. (**H**) Top 10 significantly enriched terms, ranked by their enrichment scores that are overrepresented in the 1015 proteins detected in the small EV samples by LC-MS. Values in bars indicate the number of proteins in the functional term. (**I**) Venn diagram showing the comparison of all proteins detected in the EV samples by LC-MS with proteins from the Vesiclepedia database.

24 hours were collected independent from the samples of the second 24 hours. Nanoparticle tracking analysis (NTA) established that there were no apparent time-dependent changes in distribution of EV size during 24 hours (Fig. 2, D and E). Note that the hydrodynamic size measured by NTA [173.3 ± 77 nm (SD)] is larger than TEM measurements because of hydration of the EV samples and size calculation method of NTA (*25*). The time series EVs were lysed and digested with trypsin, and the resulting peptides were purified for liquid chromatography–mass spectrometry (LC-MS). There was variation in the protein abundances between triplicates of the first 24-hour time series and between the first 24-hour and second 24-hour set of samples (Fig. 2F and fig. S1). Principal components analysis also identified that the largest source of variance was between the first and the second 24-hour time series (Fig. 2G). The LC-MS detected 1015 proteins that were supported by at least two unique peptides and in at least two samples per time point. Functional enrichment analysis revealed that the small EV proteome was overrepresented by ribosomal, vesicle, and cytoskeletal proteins, and over 90% of proteins detected mapped to proteins detected in mouse vesicles (Fig. 2, H and I). The data also showed that proteins commonly enriched in EV samples were present, including proteins that associate with EVs via lipid- or membrane protein–binding ability or promiscuous incorporation (fig. S2, A to D). Also present were proteins belonging to ribosomal subunits and secreted proteins, which are commonly recovered with EV preparations (fig. S2, E and F).

Identification of circadian EV proteins

MetaCycle (*26*) was applied to the LC-MS readouts of the complete 48-hour times series but was unable to detect any circadian rhythms. To control for variation between the first and second 24-hour time series, we then applied MetaCycle to the first 24-hour, second 24-hour, and control time series separately. Circadian rhythmic proteins were only identified in the second 24-hour time series ($q < 0.2$; Fig. 3A and data files S3 and S4). The peak phase distribution of MetaCycle-identified rhythmic proteins peaked at 22 hours after synchronization (Fig. 3B). To detect more complex circadian patterns and improve robustness to measurement noise, we applied a nonparametric Gaussian process approach that can detect repeating nonstationary oscillations with a periodicity of 22 to 26 hours (*27*). The Gaussian process model identified 106 proteins as statistically circadian-rhythmic in the 48-hour time series, of which 18 were identified in the control dataset, the latter of which were considered to be pseudocircadian and removed from further analyses (S median > 0.3, SE < 0.2; Fig. 3C, fig. S3, and data files S5 and S6). The phase distribution of peak abundance showed that the majority of proteins peaked at 23 hours after synchronization (Fig. 3D). Thirty proteins were commonly identified by the Gaussian process and MetaCycle analysis (Fig. 3E and fig. S4). Proteins that were cyclic in both analyses were reliably cyclic during 48 hours with a ~24-hour rhythmicity (fig. S5A). Proteins only cyclic in the Gaussian process analysis either exhibited a sinusoidal abundance rhythm but the triplicate data were noisy or showed a repeating nonstationary oscillation (fig. S5, A and B). Proteins only cyclic in MetaCycle analysis of the second 24-hour time series showed high variance when applied to the full 48-hour time series (fig. S5C).

Functional enrichment analysis of circadian EV proteins

Functional enrichment analysis of circadian proteins identified by both analyses revealed that RNA binding proteins and cytoskeletal (actin-binding and intermediate filaments) were overrepresented, and the peak abundances of these two groups of proteins were temporally separated at 8 hours and 22 to 23 hours after synchronization, respectively (Fig. 3, F to H). Circadian-rhythmic ECM proteins, including decorin, matrix Gla protein, periostin, and thrombospondin 2, peaked in abundance at 22 hours after synchronization (Fig. 3 I), whereas proteins involved in vesicle formation had peak abundance in small EVs between 12 and 24 hours after synchronization (Fig. 3J).

Proteomic time signatures for tendon fibroblast small EVs

Correlation analysis of Gaussian process– and MetaCycle-determined peak phases of the 30 common proteins showed a high degree of correlation, except for four proteins, alkaline phosphatase, filamin B, S100 calcium-binding protein A4, and tubulin-specific chaperone A, which have peak phases between 16 and 24 hours after synchronization (Fig. 4A). We cross-referenced the Gaussian process– and MetaCycle-identified circadian proteins with the existing dataset of rhythmic salt-soluble proteins from mouse tendon tissue (*7*) and found that 41 proteins showed commonality between at least two of these lists (Fig. 3E). As expected, most of these (30 proteins) were common between the Gaussian process– and MetaCycle-determined lists. The little overlap with the list of rhythmic salt-soluble proteins from mouse tendon tissues confirmed that most of the circadian-rhythmic EV proteins were vesicle derived and would not have been isolated by incubating tendon tissue in salt solution. Of these 41 proteins, those that showed less than 6-hour difference in time of peak abundance were used to create a circadian proteomic signature for tendon fibroblast small EVs (37 proteins) (Fig. 4B). Small EV samples at 22 hours after synchronization are enriched for proteins involved in cytoskeletal organization (plakoglobin and keratins), and small EV samples at 6 hours after synchronization are enriched for ribosomal proteins (Fig. 4C).

EV MMP14 level is regulated via endosomal sorting

In tendon fibroblasts, MMP14 plays a critical role in ECM synthesis and has potential to act via its localization in EVs (*22*–*24*). We hypothesized that MMP14 is localized to fibroblast EVs and that this localization is regulated by the endosomal sorting protein flotillin-1. We performed immuno-EM analysis on the fibroblast-derived EVs using an antibody specific to the catalytic domain of MMP14 and established that the protein was localized specifically to EVs, which were observed as areas of electron dense membrane material (Fig. 5A). We did not observe any antibody binding to areas of the grid where there was an absence of membrane material (see data file S1 for uncropped TEM images). Immunoprecipitation analyses of cell lysates showed coimmunoprecipitation of endogenous MMP14 with endogenous flotillin-1 and vice versa, suggesting the proteins have endogenous interactions (fig. S6, A to D). In synchronized fibroblast, there was time-dependent expression of flotillin-1 with ~37% difference in protein levels between time points of peak and nadir expression (fig. S6E). To mimic this nadir expression level, we used an RNA interference approach to target *Flot1* and were able to reproducibly achieve a ~40% knockdown in flotillin-1 protein in cell lysates and small EVs compared with controls (Fig. 5, B to E). Flotillins regulate each other (*28*), and Western blot analysis confirmed a ~25% reduction of flotillin-2 in siFlot1 cells and ~40% reduction in small EVs (Fig. 5, B and D, and fig. S6E). Knockdown of flotillin-1 did not affect the levels of CD9, a marker for exosome biogenesis

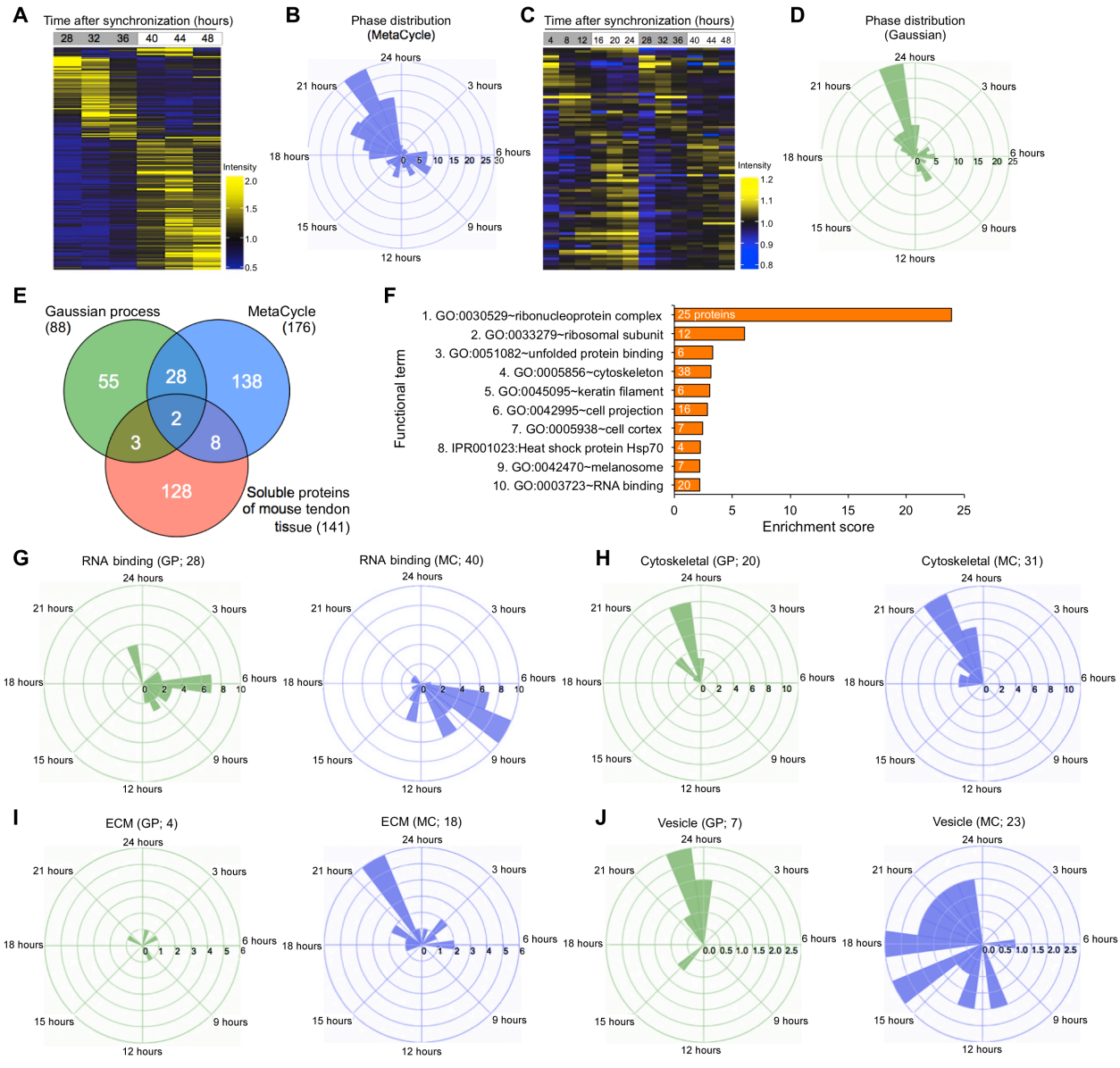

Fig. 3. Identification and phase characteristics of circadian small EV proteins. (**A**) Heatmap showing the mean expression of the 176 circadian rhythmic proteins identified by MetaCycle analysis ($q < 0.2$) in the second 24-hour dataset. (**B**) Phase distribution of peak abundances of the MetaCycle-identified rhythmic proteins. (**C**) Heatmap showing the mean expression of the 88 circadian rhythmic proteins identified by the Gaussian process (S median > 0.3, SE <0.2) in the 48-hour time series. (**D**) Phase distribution of peak abundances of the Gaussian process–identified rhythmic proteins. (**E**) Venn diagram showing the comparison of circadian small EV proteins identified by the Gaussian process and MetaCycle analysis with circadian proteins identified in the soluble fraction of mouse tendon tissue. (**F**) Top 10 significant enriched terms in circadian proteins identified by both Gaussian process and MetaCycle analyses, ranked by their enrichment scores. Values in bars indicate the number of proteins in the functional term. (**G** to **J**) Comparison of the phase distribution of peak abundances of Gaussian process–identified (GP) and MetaCycle-identified (MC) proteins belonging to ribosomal/ribonucleoprotein/RNA binding (G), cytoskeletal (H), and ECM (I) and related to vesicles/endocytosis (J) functional terms. Values in brackets indicate the number of proteins.

(Fig. 5, B and D, and fig. S6F) (*29*, *30*). Western blotting and immunofluorescence analyses showed a small but consistent increase in MMP14 in siFlot1 cell lysates, at the plasma membrane, and more apparent in small EVs (Fig. 5, B to F). To investigate whether this increase in cellular and EV MMP14 protein was due to modulated sorting in endosomes, we performed confocal microscopy and observed an increased colocalization of MMP14 staining with the early endosome marker, early endosome antigen 1 (Fig. 5, G and H). We hypothesized that in flotillin-1–depleted cells, MMP14 was not being directed toward lysosomes for degradation. To test whether MMP14 is a substrate for lysosomal degradation in tendon fibroblasts, we treated cells with a V-type adenosine triphosphatase–specific inhibitor, bafilomycin A1, to block lysosome function and observed a small but significant increase in MMP14 protein (fig. S6G). We searched the rhythmic EV proteins (88 identified by Gaussian process and 176 identified by MetaCycle) and found that ~20%

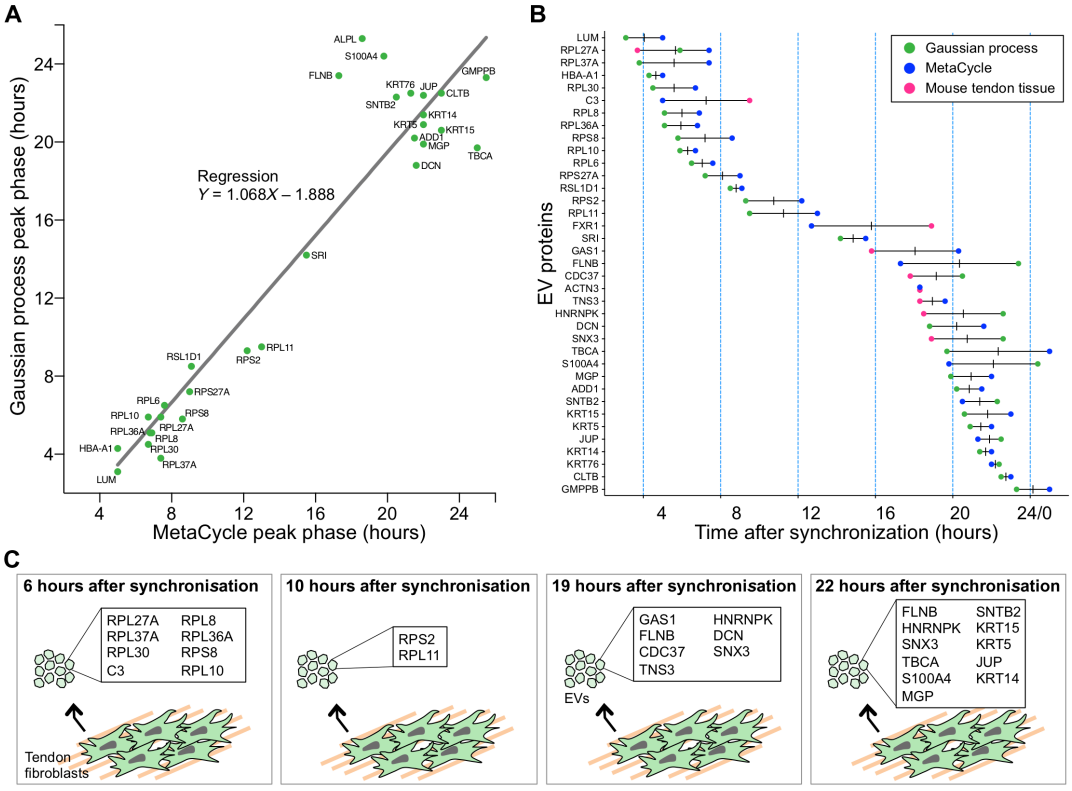

Fig. 4. Circadian periodicity analysis provides a proteomic time signature for fibroblast small EVs. (**A**) Correlation between the MetaCycle-derived peak phase and the mean peak phase derived from the Gaussian process for the 30 common proteins ($R^2 = 0.8954$). Proteins are expressed using gene names. (**B**) Pattern of peak abundance of circadian small EV proteins validated by at least two analyses with less than 6-hour peak phase time. (**C**) Schematic of how the protein composition of small EVs from healthy fibroblast changes for 24 hours.

contained a putative dileucine motif that could potentially be regulated similarly to MMP14 by flotillin-1 (data file S7).

DISCUSSION

Using label-free quantitative LC-MS–based proteomics in combination with circadian periodicity analysis, we have identified proteomic time signatures for small EVs, including exosomes, released by synchronized primary mouse tendon fibroblasts. Functional enrichment analysis of EV proteins with circadian-rhythmic abundance revealed that the release of small EVs enriched in RNA binding proteins were temporally separated to the release of small EVs enriched in ECM and cytoskeletal proteins. Last, we established that MMP14 is localized to tendon fibroblast small EVs, and its abundance in this localization is under the regulation of flotillin-1, the gene of which is strictly circadian controlled (*14*, *17*).

In this study, we have applied two independent methods to detect 24-hour periodicity in the abundance of individual EV proteins. MetaCycle uses parametric models to detect rhythmic behavior with sinusoidal patterns, but not all rhythmic behaviors are easily captured by this parametric model, especially if the time series is noisy (e.g., data from first 24-hour time series). In addition, natural circadian rhythms may fluctuate in amplitude (*31*), and estimation of rhythmicity is difficult in noisy time series data of short duration. Consequently, we additionally applied a nonparametric Gaussian process model that is optimized for detecting complex rhythms (*27*). Both approaches established that the abundance of the majority of circadian proteins in small EVs peaked at 22 to 23 hours after synchronization and that proteins belonging to different functional groups peaked at distinct times in the circadian cycle.

RNA binding proteins exhibited peak abundance between 6 and 10 hours after synchronization. RNA binding proteins were also observed previously in EVs released by human tendon fibroblasts (*32*). We reasoned that these proteins are present in EVs to form complexes with and to stabilize RNA cargo (*33*, *34*), and their peak abundance coincides with the phase of maximum expression of over 150 circadian clock–controlled genes in mouse tendons (*17*). The abundance of proteins in small EVs regulating the cytoskeleton peaked at 22 to 23 hours after synchronization. Exosomes with a comparable biochemistry have previously been demonstrated to initiate cytoskeletal rearrangement in recipient cells (*35*). Actin reorganization in cellular protrusions called fibripositors is critical for collagen fibril assembly (*36*). ECM proteins decorin, lumican (*37*), and thrombospondins (*38*, *39*) regulate collagen fibril assembly, and they were found to be enriched in small EVs at 22 hours after synchronization. Docking of EVs may help concentrate cargo proteins in cells (*40*). Together, these data lead us to hypothesize that tendon small EVs act in an autocrine manner by synchronizing cells with one another, for example, priming cells for fibril assembly when there is a simultaneous peak in procollagen type I molecules secreted into

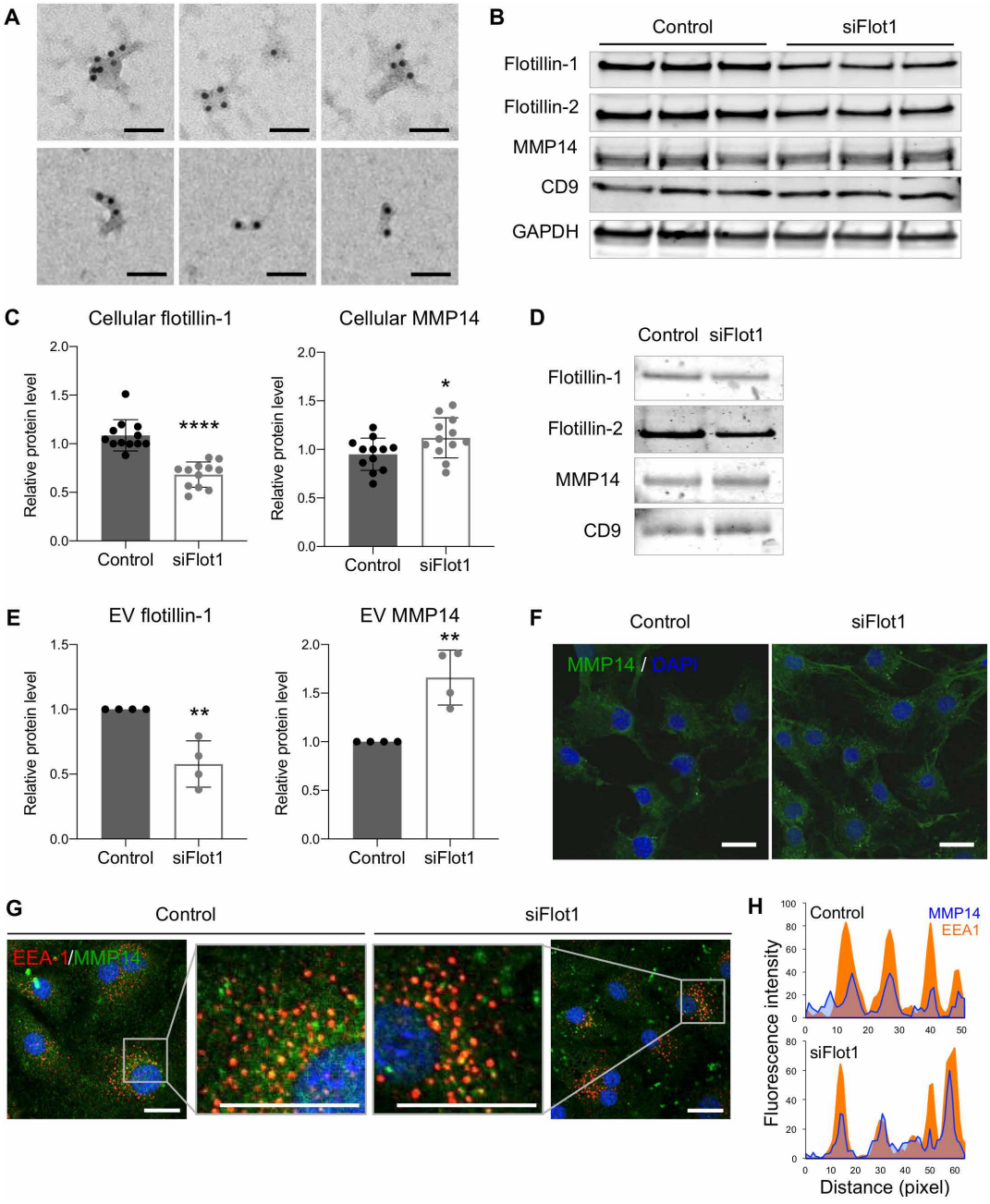

Fig. 5. EV MMP14 level is regulated via the endosomal pathway. (**A**) Representative images of immuno-EM analysis of small EVs purified from primary mouse tendon fibroblast cultures labeled with antibodies specific to the catalytic domain of MMP14 and visualized with 10-nm gold-gold particles (black dots). Scale bars, 50 nm. (**B**) Representative Western blot analysis of lysates from tenocytes treated with small interfering RNAs (siRNAs) targeting *Flot1*. (**C**) Quantification of protein levels from Western blot analysis of cellular flotillin-1 and MMP14 from control cells and cells treated with siRNAs targeting *Flot1* ($n = 3$ independent experiments, normalized to GAPDH loading control; $^{****}P < 0.0001$ and $^{*}P = 0.0371$, unpaired t tests). (**D**) Representative Western blot analysis of small EVs released by tenocytes with depleted flotillin-1. (**E**) Quantification of protein levels from Western blot analysis of EV flotillin-1 and MMP14 from control cells and cells treated with siRNAs targeting *Flot1* ($n = 4$ independent experiments, 5 μg of protein loaded; $^{**}P < 0.0032$ for flotillin-1 and $^{**}P < 0.0034$ for MMP14, unpaired t tests). (**F**) Representative confocal fluorescence microscopy images showing increased fluorescence intensity for MMP14 in flotillin-1–depleted cells. Scale bars, 20 μm. (**G**) Representative confocal fluorescence microscopy images showing increased colocalization of MMP14 with early endosomes, localized via early endosome antigen-1 (EEA-1), in cells treated with siRNAs targeting *Flot1*. Scale bars, 10 μm. (**H**) Line scan analysis of confocal images shows reduced MMP14 staining outside early endosomes. See data file S1 for original scans of Western blots and gels and uncropped TEM images.

the ECM (*7*). Functional studies examining the effects of exosome and small EVs isolated from different times of the day on ECM assembly and their mode of function would be required to test this hypothesis.

A major limitation of this study was the small amount of EV protein released during 4 hours that was analyzed for each time point. This shortfall was minimized by pooling samples from two experiments for each replicate; however, because of the small sample size, there was variation in the abundance of protein analyzed by LC-MS, so our analysis may have omitted proteins at low abundance. To be confident in the identification of circadian EV proteins, we collected samples from two circadian cycles with a 4-hour resolution, applied two complimentary statistical analyses, used stringent cutoffs, and cross-referenced the proteins identified with an existing time series proteomics dataset of soluble proteins extracted from mouse tendons (*7*). Biological rhythms are often noisy and may be overlaid with another trend, e.g., increasing or decreasing abundance. Stationary methods can reliably detect periodicity when the dataset is robust and the oscillations are stable.

In this study, the MetaCycle analysis was only able to identify circadian proteins in the second 24-hour time series, which was likely due to the batch effect of preparing the first and the second 24-hour time series for LC-MS and due to variation between triplicate samples in the first 24-hour time series. This limitation means that the circadian proteins identified cannot be extrapolated beyond the 24 hours, so there may be inconsistencies with which proteins are really circadian. The Gaussian process model, on the other hand, separates periodic signals from nonperiodic signals and considers the batch effect as the aperiodic signal to some extent. Thus, this model was able to process the full 48-hour time series and identify proteins with both sinusoidal 24-hour rhythms (in common with MetaCycle) and 24-hour rhythms with repeating behavior combined with another trend, e.g., increasing abundance. Therefore, the Gaussian process analysis of the 48-hour time series can more robustly identify circadian proteins than the MetaCycle analysis of one 24-hour data. There were only 30 proteins commonly identified in both methods, but the phase distribution and enrichment of the uncommon circadian proteins were consistent between the two analyses.

Another criticism of the study would be the experimental setup for the time series isolation of small EVs, where a response to serum withdrawal during 24 hours would generate pseudorhythmicity in EV protein abundance. To control for any serum-withdrawal response, we analyzed small EVs isolated from unsynchronized cells and eliminated any pseudocircadian proteins from further analyses. Together, we presented only a modest number of small EV proteins as circadian time signature markers.

The discrepancy in the size of EVs analyzed by TEM and NTA was due to differences in the techniques used and conditions under which the particles were analyzed and measured (*25*). For TEM, samples were fixed, dehydrated, and imaged adhered to a surface in a vacuum, all of which may cause a reduction in size (*41*). For NTA, samples were hydrated in phosphate-buffered saline (PBS), and the hydrodynamic size calculation is dependent on and highly sensitive to the viscosity and temperature of the liquid. It is common for the NTA-reported size of EVs to be larger because the diffusion of EVs is affected by their interfacial properties, which also makes it difficult to avoid even by using a standard of known particle size (*42*). Between the two methods, TEM is considered the most accurate approach for measuring EV size (*43*).

MMP14 and its substrate pro-MMP2 were overall not identified as having any rhythmic abundance in our small EV time series dataset, which can be attributed to our relatively small sample size. However, we did establish circadian rhythms in MMP14 protein level and MMP2 activation in lysates of synchronized cells, demonstrated the presence of MMP14 in small EVs, and found an association between MMP14 and flotillin-1, the latter of which we predict is via the dileucine motif of MMP14 (*22*–*24*). Flotillins can indirectly interact with ubiquitinated cargo to regulate their sorting (*44*). MMP14 contains a Lys^{581} residue that becomes monoubiquitinated, which does not lead to any degradation via the proteasome (*45*). The increase in MMP14 with bafilomycin A1 treatment suggests that some MMP14 is degraded via lysosomes. In other studies, flotillin-1 depletion led to an accumulation of a substrate that interacts via a dileucine motif (*16*) and disrupted the recycling of other substrates (*46*, *47*), whereas overexpression of flotillins led to distension of recycling compartments (*46*). Here, an RNA interference approach was taken to (i) mimic the nadir phase of flotillin-1 expression during a circadian cycle, where protein levels do not fall to zero, and to (ii) circumvent potential compensatory mechanisms as a result of gene deletion that may interfere with interpretation of data. Because of the small amount of sample, whether flotillins regulate exosome and EV abundance (biogenesis and/or release) was not investigated, but it would be an important line of study in future investigations. Together, these data suggest a mechanism whereby during a 24-hour period, MMP14 is directed for lysosomal degradation when flotillin-1 level is high and MMP14 is allowed to accumulate in membrane compartments when flotillin-1 level is low. As circadian rhythmicity of flotillin-1 is not unique to tendon (*14*), we predict that this mechanism of regulating cargo protein abundance is also present in other cell types.

In conclusion, the circadian clock regulation of rhythmic gene expression and protein abundance indirectly leads to temporal-specific loading of proteins in small EVs. Furthermore, the circadian clock–controlled expression of sorting proteins in the endosomal pathway directly mediates the abundance of targeted cargo proteins in exosomes. In tendon cells, the circadian clock–regulated small EVs coordinate ECM assembly and remodeling, and beyond tendon cell biology, these findings reveal how exosomes and other small EVs may facilitate temporal synchronization between different cells within and between tissues.

MATERIALS AND METHODS

Experimental design

The primary objective was to investigate whether there is a circadian pattern in exosome and small EV protein composition. We designed a protocol for time series small EV isolation from synchronized and control unsynchronized cells and generated data by LC-MS. The synchronization protocol was validated by real-time bioluminescence recordings, Western blotting, and zymography. EV isolation protocol was validated by Western blotting and TEM. The LC-MS data were analyzed for proteins with circadian-rhythmic abundances using two statistical approaches. The secondary objective was to investigate whether flotillin-1 regulates MMP14 in small EVs of tendon fibroblasts. To this end, an RNA interference approach was taken. Data were generated by immuno-EM of small EVs,

immunoprecipitation on cell extracts, Western blotting on cell and EV extracts, and immunofluorescence on fixed cells. For all experiments, replicate numbers are outlined in Materials and Methods or figure legends. Minimum sample size was $n = 3$ different preparations of cells for each experiment. Experimenters were not blinded to experimental groups, but where possible, automated analysis was used to remove bias. The care and use of all mice in this study were carried out in accordance with the law on animal experiments in Denmark (Law on Animal Experiments in Denmark, LBK nr. 474, 15 May 2014) and Directive 2010/63/EU with the license number 2017-15-0201-01364 issued to J.H. from the Animal Inspectorate, Ministry of Food, Agriculture and Fisheries, Denmark. No experiments were performed on live animals.

Mouse tendon fibroblasts

Primary mouse tail tendon fibroblasts were released from mouse tail tendons of *PER2::Luciferase* mice (*48*), aged between 6 and 8 weeks old, by incubating tendons overnight in collagenase type 2 (400 U/ml; Worthington Biochemical Corporation) prepared in Dulbecco's modified Eagle's medium/Ham's F-12 medium (DMEM/F-12) (without phenol red; Thermo Fisher Scientific) supplemented with 20% fetal calf serum (FCS; S181H-500, Biowest) and penicillin (50 U/ml) and streptomycin (50 μg/ml; Thermo Fisher Scientific) at 37°C in 5% CO_2. After, cells were strained through a 70-μm filter (BD Biosciences) and centrifuged for 6 min at 600*g*. All cells were cultured in complete medium [DMEM/F-12 medium supplemented with 10% FCS and penicillin (50 U/ml) and streptomycin (50 μg/ml)] at 37°C in 5% CO_2. Cells were passaged 1 in 3 when 70 to 80% confluent. Cells between passages 2 and 4 were used in the experiments. For the blockade of lysosome function, cells were treated with 200 nM bafilomycin A1 for 2 hours in serum-free medium at 37°C in 5% CO_2.

Synchronization of cell cultures

Synchronization of cells was achieved by incubation with 100 nM dexamethasone (Sigma-Aldrich) diluted in complete medium for 24 hours at 37°C in 5% CO_2. Control cells were incubated with fresh complete medium for 24 hours at 37°C in 5% CO_2. After, at 0 hour after synchronization, cells were washed with PBS three times. Cells were then incubated with serum-free, CO_2-independent medium [DMEM/F-12 supplemented with 0.035% sodium bicarbonate (Sigma-Aldrich), 10 mM Hepes (Sigma-Aldrich), 1× GlutaMAX supplement (Thermo Fisher Scientific), and penicillin (50 U/ml) and streptomycin (50 μg/ml)] at 37°C in 5% CO_2. For 24-hour time series small EV isolations, cells in three T225 flasks were used per experiment (10 ml of serum-free, CO_2-independent medium per flask). Every 4 hours during the 24 hours, the conditioned medium was collected for small EV isolation, and fresh serum-free, CO_2-independent medium was replaced on the cells.

RNA interference

For transient knockdown experiments, cells were transfected with 5 nM Silencer-Select Pre-Designed small interfering RNAs (siRNAs) targeting mouse *Flot1* mRNA NM_008027.2 (siRNA IDs s66143 and s66145, Thermo Fisher Scientific) using Lipofectamine RNAiMAX (Thermo Fisher Scientific). Controls were treated with transfection reagent only. Complete medium was replaced after 24 hours for 24 hours. After, cells were incubated with serum-free, CO_2-independent medium for 16 hours (64 hours from transfection).

Real-time bioluminescence recording

Synchronized *PER2::Luciferase* cells grown in glass bottom 35-mm dishes (Ibidi) were cultured with recording medium [0.1 mM D-luciferin (Sigma-Aldrich) in DMEM/F-12 supplemented with 5% FCS, 0.035% sodium bicarbonate (Sigma-Aldrich), 10 mM Hepes (Sigma-Aldrich), 1× GlutaMAX supplement (Thermo Fisher Scientific), and penicillin (50 U/ml) and streptomycin (50 μg/ml)] at 37°C in 5% CO_2. AB-2550 Kronos Dio (ATTO) and ATTO Dish Type Luminescence Kronos v2.10.231 software were used for real-time quantitative bioluminescence recording at 37°C in 5% CO_2. Baseline subtraction was carried out using a 24-hour moving average. Period was calculated using RAP v1.0 algorithm (*49*). Mean and SD were calculated.

Small EV isolation and purification

Conditioned medium was ultrafiltered through a 0.22-μm filter (Sartorius) to remove any intact cells and then centrifuged at 2000*g* for 20 min at 4°C to remove cell debris. The supernatant was further centrifuged at 4566*g* for 1 hour at 4°C. The supernatant was ultracentrifuged in 5-ml polypropylene centrifuge tubes (Beckman Coulter) at 100,000*g* for 2 hours at 4°C using an SW 55 Ti rotor and Optima L-80 XP Ultracentrifuge (Beckman Coulter). The pellet containing crude EV extract was resuspended in 40 μl of BioUltra PBS (Sigma-Aldrich) and then mixed with 335 μl of 90% sucrose (Sigma-Aldrich) in BioUltra PBS (final concentration, 82%). The suspension was overlaid with a decreasing sucrose gradient (3775 μl of each 70, 64, 58, 52, 46, 40, 34, 28, 22, 16, and 10%) in polypropylene centrifuge tubes and ultracentrifuged at 100,000*g* for 16 hours at 4°C. The fraction containing the 34 and 40% sucrose was enriched for exosomes and small microvesicles, and this was diluted with 4 ml of BioUltra PBS and ultracentrifuged at 100,000*g* for 1 hour at 4°C.

Western blotting

Cells were lysed with ice-cold radioimmunoprecipitation assay (RIPA) buffer (Sigma-Aldrich) containing protease and phosphatase inhibitors (Roche) for 10 min on ice, vortexed briefly, and cleared by centrifugation at 10,000*g* at 4°C. Protein concentrations from cells were determined using a Pierce BCA protein assay kit (Thermo Scientific). EV pellets resulting from ultracentrifugation of the 34 and 40% sucrose fractions from each experiment were resuspended in equal volume (20 μl) of ice-cold RIPA buffer containing protease and phosphatase inhibitors. Lysates (20 μg) or EV extracts (5 μg) were reduced in sample buffer containing reducing agent and separated in 4 to 12% Criterion XT Bis-Tris gels (Bio-Rad) in XT running buffer (Bio-Rad). Proteins were transferred onto 0.45-μm low-fluorescence polyvinylidene difluoride membranes (Bio-Rad). Membranes were blocked with 20% Odyssey blocking buffer (LI-COR) in tris-buffered saline (TBS) and then incubated overnight at 4°C in primary antibodies diluted in 10% Odyssey blocking buffer in TBS. Primary antibodies used were as follows: caveolin-1 (ab17052, Abcam), CD9 (ab92726, Abcam), flotillin-1 (610820, BD Biosciences), glyceraldehyde-3-phosphate dehydrogenase (AM4300, Thermo Fisher Scientific), histone 3 (AHO1432, Thermo Fisher Scientific), HSP47 (sc-8352, Santa Cruz Biotechnology), integrin α2 (sc-74466, Santa Cruz Biotechnology), integrin α5 (sc-17029, Santa Cruz Biotechnology), integrin β_1 (ab52971, Abcam), MMP14 (ab51074, Abcam), and RNA polymerase II (ab5131, Abcam). After, membranes were washed in TBS containing 0.1% Tween 20 (TBST) and then incubated in secondary antibodies, infrared 680–conjugated goat anti-mouse (A21057, Thermo Fisher Scientific) and DyLight 800–conjugated

goat anti-rabbit (35571, Pierce), diluted in 10% Odyssey blocking buffer in TBST for 1 hour at room temperature (RT). Immunoreactive bands were captured using a LI-COR Odyssey scanner and LI-COR Odyssey software or a LI-COR Fc Imager and Image Studio v5.2.5. Quantification of Western blot bands was performed using Fiji (*50*). Original scans of Western blots can be found in data file S1.

Immunoprecipitation

Cells were lysed with ice-cold immunoprecipitation buffer [10 mM tris-HCl (pH 8.0), 150 mM NaCl, 5 mM EDTA, 0.5% Triton X-100, 60 mM *n*-octyl-β-D-glucopyranoside (Sigma-Aldrich)] containing protease and phosphatase inhibitors. Protein concentrations from cells were determined using Quick Start Bradford Protein Assay reagent (Bio-Rad). Protein (3 to 4 mg/ml) in immunoprecipitation buffer was incubated with control rabbit immunoglobulin G (10 μg/ml; Thermo Fisher Scientific) or monoclonal antibodies to flotillin-1 (ab133497, Abcam) or MMP14 (ab51074, Abcam) overnight on a vertical rotator at 4°C. After, protein G agarose beads (100 μl/ml; Roche) were added and incubated for a further hour. Bound protein complexes were spun down, washed twice with immunoprecipitation buffer and once with 1× TBS, and eluted by heating in 4× Laemmli sample buffer (Bio-Rad) containing reducing agent (Bio-Rad) for 10 min at 95°C for analysis by Western blotting.

Immunofluorescence

Cells grown on glass coverslips were fixed with Histofix (Histolab) for 10 min at RT and then washed with TBS three times. Cells were blocked and permeabilized with 0.3% Triton X-100 and 1% bovine serum albumin (BSA) in TBS for 1 hour at RT and then incubated in primary antibodies to MMP14 (clone LEM-2763.1; ab78738, Abcam) and early endosome antigen-1 (clone C45B10; 3288T, Cell Signaling Technology) overnight at 4°C. After washing, coverslips were then incubated with secondary antibodies Alexa Fluor 488–conjugated goat anti-mouse (A11031, Thermo Fisher Scientific) and Alexa Fluor 568–conjugated goat anti-rabbit (A11034, Thermo Fisher Scientific) for 1 hour at RT. After washing, coverslips were mounted with ProLong Gold Antifade Mountant with DAPI (Thermo Fish Scientific). All fluorescence images were collected by laser scanning confocal microscopy (SP5-X; Leica) with Leica Application Suite software (version 2.7.3.9723), using a ×63 immersion (water) objective. Images were collected with the same settings for control and treated cells. Image analyses were performed using Fiji (*50*).

Gelatin zymography

Protein lysates (10 μg) were incubated with nonreducing 2× Novex tris-glycine SDS sample buffer (Thermo Fisher Scientific) for 30 min at RT and then separated in Novex 10% gelatin protein gels (Thermo Fisher Scientific) in 1× Novex tris-glycine SDS running buffer (Thermo Fisher Scientific). After electrophoresis, the gels were washed twice for 15 min at RT with 1× Novex renaturing buffer (Thermo Fisher Scientific) and then washed for 30 min at RT with 1× Novex developing buffer (Thermo Fisher Scientific). After the gels were incubated with fresh developing buffer for 2 days at 37°C, the gels were stained with Coomassie blue for 1 hour at RT. The gels were destained in 30% methanol until the bands appeared. Quantification of digested bands from scanned gels was performed using Fiji (*50*). Original scans of gels can be found in data file S1.

Electron microscopy

TEM analysis of tendon fibroblasts in three-dimensional tendon constructs was performed as described previously (*51*). TEM, analysis of small EVs were prepared as previously described (*32*). EV pellets were resuspended and fixed in 2% glutaraldehyde in 100 mM phosphate buffer. Fixed EVs were mounted onto copper grids (Agar Scientific), then stained with 1% (w/v) uranyl acetate (Sigma-Aldrich) in ddH_2O for 3 min at RT, and washed with ddH_2O. For immuno-EM for MMP14, small EV extracts were resuspended in ice-cold PBS containing protease and phosphatase inhibitors. Without fixation, the small EVs were mounted onto copper grids covered with a continuous carbon film. All steps were performed at RT with care not to dry out the samples. The small EVs were blocked with 0.1 M PBS containing 50 mM glycine, 1% BSA, 0.2% Tween-20, and 0.1% sodium azide for 10 min two times. After, a mouse monoclonal antibody raised against amino acid sequence 218 to 233 within the catalytic domain of MMP14 (clone LEM-2/15.8; MAB3328, Merck), which we have validated previously for immuno-EM and shows no immunoreactivity in MMP14-null mouse tissues (*18*), was applied for 20 min at RT. After washing with blocking buffer for 10 min three times, 10-nm gold-conjugated protein A (R14049-1, Agar Scientific) was applied for 20 min. The grids were then washed with blocking buffer for 10 min twice, followed by washes in ddH_2O for 2 min six times. After, the grids were stained with 1% uranyl acetate in ddH_2O for 3 min and washed with ddH_2O. Grids were examined with a Tecnai 12 instrument (FEI) fitted with a 2 k × 2 k–cooled Teitz F214A charge-coupled device camera (Tietz Video and Image Processing Systems). Images were taken at ×13,000 magnification for EV diameter measurements using Fiji (*50*). Mean and SD were calculated.

Nanoparticle tracking analysis

EV pellets resulting from ultracentrifugation of the 34 and 40% sucrose fractions from each experiment were resuspended in 500 μl of particle-free BioUltra PBS. Samples were measured and quantified using a NanoSight LM10 running NTA v3.1 software (Malvern, UK). Immediate prior to measurement small EV suspensions were vortexed at high speed for 10 s to break up any aggregates. An average of 17.4 ± 10 particles per frame was measured. Data were collected from standard measurement recorded at 20° to 22°C with viscosity set to water (0.940 to 0.948 centipoise), camera level to 16, and detection threshold to 4, and all other parameters were set as default. Each standard measurement included five videos with duration of 1 min (5 min in total), and fresh sample was injected for measurement before each video. The sum of hydrodynamic size distribution of valid tracks from five videos was used for each time point.

Time series small EV protein isolation

In our experimental setup, samples were isolated independently for each 24-hour time series, i.e., samples for 4, 8, 12, 16, 20, and 24 hours after synchronization were isolated from one experiment, and samples for 28, 32, 36, 40, 44, and 48 hours after synchronization were isolated from another experiment. For each set of time series samples [4 to 24 hours (n = 3), 28 to 48 hours (n = 3), and control 4 to 24 hours (n = 3)], isolates from two independent experiments were pooled together for sufficient material for analysis. EV pellets resulting from ultracentrifugation of the 34 and 40% sucrose fractions from each experiment were resuspended and lysed with 6 M guanidine hydrochloride, 10 mM tris (2-carboxyethyl) phosphine

hydrochloride, 40 mM 2-chloroacetamide, and 100 mM tris (pH 8.5) for MS analysis. Protein concentrations were determined by Quick Start Bradford Protein Assay (Bio-Rad) according to the manufacturer's instructions.

Tryptic digestion of EV proteins and LC-MS

EV proteins were digested for LC-MS as described previously (*32*). Samples for the first 24-hour, second 24-hour, and control time series were processed in three batches. For each sample, 500 ng of peptides was loaded onto a 2-cm C18 trap column (Thermo Fisher Scientific), connected in-line to a 50-cm C18 reverse-phase analytical column (EASY-Spray LC column, Thermo Fisher Scientific) using 0.1% formic acid in water at 750 bar, using the EASY-nLC 1200 high-performance LC system (Thermo Fisher Scientific) and the column oven operating at 45°C. Peptides were eluted over a 140-min gradient ranging from 6% to 60% of 80% acetonitrile and 0.1% formic acid at 250 nl/min, and the Orbitrap Fusion instrument (Thermo Fisher Scientific) was run in a data-dependent MS/MS (DD-MS2) top speed method. Full MS spectra were collected at a resolution of 120,000, with an automatic gain control (AGC) target of 4×10^5 or maximum injection time of 50 ms and a scan range of 400 to 1500 mass/charge ratio (m/z). The MS2 spectra were obtained in the ion trap operating at rapid speed, with an AGC target value of 1×10^4 or maximum injection time of 35 ms, a normalized higher-energy collisional dissociation collision energy of 30, and an intensity threshold of 1.7×10^4. Dynamic exclusion was set to 60 s, and ions with a charge state <2, >7, or unknown were excluded. MS performance was verified for consistency by running complex cell lysate quality control standards, and chromatography was monitored to check for reproducibility.

Label-free quantitative proteomics analysis

The MS proteomics data have been deposited to the ProteomeXchange Consortium via the PRIDE partner repository (www.ebi.ac.uk/pride/archive/) with the dataset identifier PXD022393. The raw files were analyzed using Proteome Discoverer 2.4. Label-free quantitation was enabled in the processing and consensus steps, and spectra were matched against the *Mus musculus* validated databases obtained from UniProt. Dynamic modifications were set as oxidation (M), deamidation (N,Q), and acetyl on protein N termini. Cysteine carbamidomethyl was set as a static modification. All results were filtered to a 1% false discovery rate (FDR), and protein quantitation was done using the built-in Minora Feature Detector. Only proteins for which two unique peptides were detected were analyzed. Proteins suggested by the Minimal Information of Studies for EVs 2018 (*52*) were used for protein content–based EV characterization.

Rhythmic protein identification

Periodicity analyses were applied to proteins that were detected in at least two of the triplicate samples per time point. MetaCycle (*26*) was applied to the LC-MS readouts of the full 48-hour time series and then, separately, the first 24-hour, second 24-hour, and control time series. JTK and Lomb-Scargle methods were selected. Circadian rhythmic proteins were only identified in the second 24-hour time series. Data files S3 and S4 contain the readouts of the MetaCycle analyses for the second 24-hour and control time series, respectively, where a Benjamini-Hochberg FDR less than 0.2 was used to identify rhythmic proteins. Circadian periodicity of EV proteins were analyzed using an approach previously described by Durrande *et al.* (*27*). Briefly, a Gaussian process model was fitted to each protein time series (full 48 hours), where the kernel is composed of a periodic and nonperiodic part. The periodicity of the time series was estimated using the S statistics, which quantifies the amount of variance explained by the periodic part of the kernel: $S = \frac{\mathrm{Var}_R[y_p(R)]}{\mathrm{Var}_R[y_p(R)+y_a(R)]}$, where y_p and y_a are the periodic and aperiodic predictions from the Gaussian process given the data over the range R. Proteins with a median of S greater than 0.3 with an SE less than 0.2 were statistically circadian rhythmic. Data files S5 and S6 contain the results for the 48-hour time series and control time series, respectively. To perform the same analysis as the 48-hour time series on the control time series that has a 24-hour length, the control data were combined with the second 24-hour time series data to provide a 48-hour dataset. Functional enrichment analysis was performed using the online tool DAVID version 6.7 (*53*). Proteins with putative dileucine motifs DxxLL were identified using the online Expasy ScanProsite tool at https://prosite.expasy.org/scanprosite/ (data file S7).

Statistical analysis

Mean, SD, and SEM were calculated for datasets from at least three independent experiments (n numbers are indicated in figure legends). SEM bars are plotted where $n \geq 3$. Where $n < 2$, a note is made in the figure or figure legend. Cellular protein data were evaluated using unpaired t tests, and EV protein data were evaluated using paired t tests using Prism 5 (GraphPad Prism Software). Significant differences are indicated in the figure legends. Analyses of variation between EV LC-MS samples (first 24 hours, $n = 3$; second 24 hours, $n = 3$; and control, $n = 3$) were performed using the R-based integrated web application Differential Expression and Pathway version 0.90 (*54*). For NTA, the lower and upper quartiles and the median were calculated. Two-way analysis of variance (ANOVA) showed no significant differences between time points.

SUPPLEMENTARY MATERIALS

Supplementary material for this article is available at https://science.org/doi/10.1126/sciadv.abc9061

View/request a protocol for this paper from *Bio-protocol*.

REFERENCES AND NOTES

1. J. Bass, M. A. Lazar, Circadian time signatures of fitness and disease. *Science* **354**, 994–999 (2016).
2. T. Roenneberg, M. Merrow, The circadian clock and human health. *Curr. Biol.* **26**, R432–R443 (2016).
3. A. Balsalobre, S. A. Brown, L. Marcacci, F. Tronche, C. Kellendonk, H. M. Reichardt, G. Schutz, U. Schibler, Resetting of circadian time in peripheral tissues by glucocorticoid signaling. *Science* **289**, 2344–2347 (2000).
4. N. P. Hoyle, E. Seinkmane, M. Putker, K. A. Feeney, T. P. Krogager, J. E. Chesham, L. K. Bray, J. M. Thomas, K. Dunn, J. Blaikley, J. S. O'Neill, Circadian actin dynamics drive rhythmic fibroblast mobilization during wound healing. *Sci. Transl. Med.* **9**, eaal2774 (2017).
5. G. Artiushin, S. L. Zhang, H. Tricoire, A. Sehgal, Endocytosis at the drosophila blood-brain barrier as a function for sleep. *eLife* **7**, (2018).
6. M. S. Robles, J. Cox, M. Mann, In-vivo quantitative proteomics reveals a key contribution of post-transcriptional mechanisms to the circadian regulation of liver metabolism. *PLOS Genet.* **10**, e1004047 (2014).
7. J. Chang, R. Garva, A. Pickard, C. C. Yeung, V. Mallikarjun, J. Swift, D. F. Holmes, B. Calverley, Y. Lu, A. Adamson, H. Raymond-Hayling, O. Jensen, T. Shearer, Q. J. Meng, K. E. Kadler, Circadian control of the secretory pathway maintains collagen homeostasis. *Nat. Cell Biol.* **22**, 74–86 (2020).
8. S. Koyanagi, A. M. Hamdan, M. Horiguchi, N. Kusunose, A. Okamoto, N. Matsunaga, S. Ohdo, Camp-response element (cre)-mediated transcription by activating transcription factor-4 (atf4) is essential for circadian expression of the period2 gene. *J. Biol. Chem.* **286**, 32416–32423 (2011).

9. A. Pickard, J. Chang, N. Alachkar, B. Calverley, R. Garva, P. Arvan, Q. J. Meng, K. E. Kadler, Preservation of circadian rhythms by the protein folding chaperone, bip. *FASEB J.* **33**, 7479–7489 (2019).
10. D. Ma, S. Panda, J. D. Lin, Temporal orchestration of circadian autophagy rhythm by C/EBPβ. *EMBO J.* **30**, 4642–4651 (2011).
11. G. Huang, F. Zhang, Q. Ye, H. Wang, The circadian clock regulates autophagy directly through the nuclear hormone receptor Nr1d1/Rev-erbα and indirectly via Cebpb/(C/ebpβ) in zebrafish. *Autophagy* **12**, 1292–1309 (2016).
12. J. Kowal, M. Tkach, C. Thery, Biogenesis and secretion of exosomes. *Curr. Opin. Cell Biol.* **29**, 116–125 (2014).
13. G. van Niel, G. D'Angelo, G. Raposo, Shedding light on the cell biology of extracellular vesicles. *Nat. Rev. Mol. Cell Biol.* **19**, 213–228 (2018).
14. R. Zhang, N. F. Lahens, H. I. Ballance, M. E. Hughes, J. B. Hogenesch, A circadian gene expression atlas in mammals: Implications for biology and medicine. *Proc. Natl. Acad. Sci. U.S.A.* **111**, 16219–16224 (2014).
15. M. Meister, R. Tikkanen, Endocytic trafficking of membrane-bound cargo: A flotillin point of view. *Membranes* **4**, 356–371 (2014).
16. B. A. John, M. Meister, A. Banning, R. Tikkanen, Flotillins bind to the dileucine sorting motif of β-site amyloid precursor protein-cleaving enzyme 1 and influence its endosomal sorting. *FEBS J.* **281**, 2074–2087 (2014).
17. C.-Y. Yeung, N. Gossan, Y. Lu, A. Hughes, J. J. Hensman, M. L. Bayer, M. Kjaer, K. E. Kadler, Q.-J. Meng, Gremlin-2 is a bmp antagonist that is regulated by the circadian clock. *Sci. Rep.* **4**, 5183 (2015).
18. S. H. Taylor, C. Y. Yeung, N. S. Kalson, Y. Lu, P. Zigrino, T. Starborg, S. Warwood, D. F. Holmes, E. G. Canty-Laird, C. Mauch, K. E. Kadler, Matrix metalloproteinase 14 is required for fibrous tissue expansion. *eLife* **4**, e09345 (2015).
19. K. Holmbeck, P. Bianco, J. Caterina, S. Yamada, M. Kromer, S. A. Kuznetsov, M. Mankani, P. G. Robey, A. R. Poole, I. Pidoux, J. M. Ward, H. Birkedal-Hansen, Mt1-mmp-deficient mice develop dwarfism, osteopenia, arthritis, and connective tissue disease due to inadequate collagen turnover. *Cell* **99**, 81–92 (1999).
20. T. Ludwig, S. M. Theissen, M. J. Morton, M. J. Caplan, The cytoplasmic tail dileucine motif ll572 determines the glycosylation pattern of membrane-type 1 matrix metalloproteinase. *J. Biol. Chem.* **283**, 35410–35418 (2008).
21. T. Uekita, Y. Itoh, I. Yana, H. Ohno, M. Seiki, Cytoplasmic tail-dependent internalization of membrane-type 1 matrix metalloproteinase is important for its invasion-promoting activity. *J. Cell Biol.* **155**, 1345–1356 (2001).
22. J. Hakulinen, L. Sankkila, N. Sugiyama, K. Lehti, J. Keski-Oja, Secretion of active membrane type 1 matrix metalloproteinase (mmp-14) into extracellular space in microvesicular exosomes. *J. Cell. Biochem.* **105**, 1211–1218 (2008).
23. H. Ngora, U. M. Galli, K. Miyazaki, M. Zöller, Membrane-bound and exosomal metastasis-associated c4.4a promotes migration by associating with the alpha(6)beta(4) integrin and mt1-mmp. *Neoplasia* **14**, 95 (2012).
24. K. Y. Han, J. Dugas-Ford, M. Seiki, J. H. Chang, D. T. Azar, Evidence for the involvement of mmp14 in mmp2 processing and recruitment in exosomes of corneal fibroblasts. *Invest. Ophthalmol. Vis. Sci.* **56**, 5323 (2014).
25. V. S. Chernyshev, R. Rachamadugu, Y. H. Tseng, D. M. Belnap, Y. Jia, K. J. Branch, A. E. Butterfield, L. F. Pease 3rd, P. S. Bernard, M. Skliar, Size and shape characterization of hydrated and desiccated exosomes. *Anal. Bioanal. Chem.* **407**, 3285–3301 (2015).
26. G. Wu, R. C. Anafi, M. E. Hughes, K. Kornacker, J. B. Hogenesch, Metacycle: An integrated r package to evaluate periodicity in large scale data. *Bioinformatics* **32**, 3351–3353 (2016).
27. N. Durrande, J. Hensman, M. Rattray, N. D. Lawrence, Detecting periodicities with gaussian processes. *PeerJ Comput. Sci.* **2**, e50 (2016).
28. T. Babuke, M. Ruonala, M. Meister, M. Amaddii, C. Genzler, A. Esposito, R. Tikkanen, Hetero-oligomerization of reggie-1/flotillin-2 and reggie-2/flotillin-1 is required for their endocytosis. *Cell. Signal.* **21**, 1287–1297 (2009).
29. K. O. Boker, N. Lemus-Diaz, R. Rinaldi Ferreira, L. Schiller, S. Schneider, J. Gruber, The impact of the cd9 tetraspanin on lentivirus infectivity and exosome secretion. *Mol. Ther.* **26**, 634–647 (2018).
30. L. T. Schiller, N. Lemus-Diaz, R. Rinaldi Ferreira, K. O. Boker, J. Gruber, Enhanced production of exosome-associated aav by overexpression of the tetraspanin cd9. *Mol. Ther. Methods Clin. Dev.* **9**, 278–287 (2018).
31. R. Refinetti, Non-stationary time series and the robustness of circadian rhythms. *J. Theor. Biol.* **227**, 571–581 (2004).
32. C. Y. C. Yeung, E. M. Schoof, M. Tamas, A. L. Mackey, M. Kjaer, Proteomics identifies differences in fibrotic potential of extracellular vesicles from human tendon and muscle fibroblasts. *Cell Commun. Signal.* **18**, 177 (2020).
33. L. Statello, M. Maugeri, E. Garre, M. Nawaz, J. Wahlgren, A. Papadimitriou, C. Lundqvist, L. Lindfors, A. Collen, P. Sunnerhagen, M. Ragusa, M. Purrello, C. Di Pietro, N. Tigue, H. Valadi, Identification of rna-binding proteins in exosomes capable of interacting with different types of rna: Rbp-facilitated transport of rnas into exosomes. *PLOS ONE* **13**, e0195969 (2018).
34. E. Willms, H. J. Johansson, I. Mager, Y. Lee, K. E. Blomberg, M. Sadik, A. Alaarg, C. I. Smith, J. Lehtio, S. El Andaloussi, M. J. Wood, P. Vader, Cells release subpopulations of exosomes with distinct molecular and biological properties. *Sci. Rep.* **6**, 22519 (2016).
35. Z. Chen, L. Yang, Y. Cui, Y. Zhou, X. Yin, J. Guo, G. Zhang, T. Wang, Q. Y. He, Cytoskeleton-centric protein transportation by exosomes transforms tumor-favorable macrophages. *Oncotarget* **7**, 67387–67402 (2016).
36. E. G. Canty, T. Starborg, Y. Lu, S. M. Humphries, D. F. Holmes, R. S. Meadows, A. Huffman, E. T. O'Toole, K. E. Kadler, Actin filaments are required for fibripositor-mediated collagen fibril alignment in tendon. *J. Biol. Chem.* **281**, 38592–38598 (2006).
37. P. J. Neame, C. J. Kay, D. J. McQuillan, M. P. Beales, J. R. Hassell, Independent modulation of collagen fibrillogenesis by decorin and lumican. *Cell. Mol. Life Sci.* **57**, 859–863 (2000).
38. S. Rosini, N. Pugh, A. M. Bonna, D. J. S. Hulmes, R. W. Farndale, J. C. Adams, Thrombospondin-1 promotes matrix homeostasis by interacting with collagen and lysyl oxidase precursors and collagen cross-linking sites. *Sci. Signal.* **11**, eaar2566 (2018).
39. P. Bornstein, T. R. Kyriakides, Z. Yang, L. C. Armstrong, D. E. Birk, Thrombospondin 2 modulates collagen fibrillogenesis and angiogenesis. *J. Investig. Dermatol. Symp. Proc.* **5**, 61–66 (2000).
40. M. Mathieu, L. Martin-Jaular, G. Lavieu, C. Thery, Specificities of secretion and uptake of exosomes and other extracellular vesicles for cell-to-cell communication. *Nat. Cell Biol.* **21**, 9–17 (2019).
41. E. van der Pol, F. A. Coumans, A. E. Grootemaat, C. Gardiner, I. L. Sargent, P. Harrison, A. Sturk, T. G. van Leeuwen, R. Nieuwland, Particle size distribution of exosomes and microvesicles determined by transmission electron microscopy, flow cytometry, nanoparticle tracking analysis, and resistive pulse sensing. *J. Thromb. Haemost.* **12**, 1182–1192 (2014).
42. Z. Varga, B. Feher, D. Kitka, A. Wacha, A. Bota, S. Berenyi, V. Pipich, J. L. Fraikin, Size measurement of extracellular vesicles and synthetic liposomes: The impact of the hydration shell and the protein corona. *Colloids Surf. B Biointerfaces* **192**, 111053 (2020).
43. S. Cavallaro, P. Hååg, K. Viktorsson, A. Krozer, K. Fogel, R. Lewensohn, J. Linnros, A. Dev, Comparison and optimization of nanoscale extracellular vesicle imaging by scanning electron microscopy for accurate size-based profiling and morphological analysis. *Nanoscale Adv.* **3**, 3053–3063 (2021).
44. M. Meister, S. Banfer, U. Gartner, J. Koskimies, M. Amaddii, R. Jacob, R. Tikkanen, Regulation of cargo transfer between escrt-0 and escrt-i complexes by flotillin-1 during endosomal sorting of ubiquitinated cargo. *Oncogenesis* **6**, e344 (2017).
45. P. A. Eisenach, P. C. de Sampaio, G. Murphy, C. Roghi, Membrane type 1 matrix metalloproteinase (mt1-mmp) ubiquitination at lys581 increases cellular invasion through type i collagen. *J. Biol. Chem.* **287**, 11533–11545 (2012).
46. G. P. Solis, N. Hulsbusch, Y. Radon, V. L. Katanaev, H. Plattner, C. A. Stuermer, Reggies/flotillins interact with rab11a and snx4 at the tubulovesicular recycling compartment and function in transferrin receptor and e-cadherin trafficking. *Mol. Biol. Cell* **24**, 2689–2702 (2013).
47. G. P. Solis, Y. Schrock, N. Hulsbusch, M. Wiechers, H. Plattner, C. A. Stuermer, Reggies/flotillins regulate e-cadherin-mediated cell contact formation by affecting egfr trafficking. *Mol. Biol. Cell* **23**, 1812–1825 (2012).
48. S. H. Yoo, S. Yamazaki, P. L. Lowrey, K. Shimomura, C. H. Ko, E. D. Buhr, S. M. Siepka, H. K. Hong, W. J. Oh, O. J. Yoo, M. Menaker, J. S. Takahashi, Period2::Luciferase real-time reporting of circadian dynamics reveals persistent circadian oscillations in mouse peripheral tissues. *Proc. Natl. Acad. Sci. U.S.A.* **101**, 5339–5346 (2004).
49. K. Okamoto, K. Onai, M. Ishiura, Rap, an integrated program for monitoring bioluminescence and analyzing circadian rhythms in real time. *Anal. Biochem.* **340**, 193–200 (2005).
50. J. Schindelin, I. Arganda-Carreras, E. Frise, V. Kaynig, M. Longair, T. Pietzsch, S. Preibisch, C. Rueden, S. Saalfeld, B. Schmid, J. Y. Tinevez, D. J. White, V. Hartenstein, K. Eliceiri, P. Tomancak, A. Cardona, Fiji: An open-source platform for biological-image analysis. *Nat. Methods* **9**, 676–682 (2012).
51. A. Herchenhan, M. L. Bayer, P. Eliasson, S. P. Magnusson, M. Kjaer, Insulin-like growth factor i enhances collagen synthesis in engineered human tendon tissue. *Growth Horm. IGF Res.* **25**, 13–19 (2015).
52. C. Thery, K. W. Witwer, E. Aikawa, M. J. Alcaraz, J. D. Anderson, R. Andriantsitohaina, A. Antoniou, T. Arab, F. Archer, G. K. Atkin-Smith, D. C. Ayre, J. M. Bach, D. Bachurski, H. Baharvand, L. Balaj, S. Baldacchino, N. N. Bauer, A. A. Baxter, M. Bebawy, C. Beckham, A. B. Zavec, A. Benmoussa, A. C. Berardi, P. Bergese, E. Bielska, C. Blenkiron, S. Bobis-Wozowicz, E. Boilard, W. Boireau, A. Bongiovanni, F. E. Borras, S. Bosch, C. M. Boulanger, X. Breakefield, A. M. Breglio, M. A. Brennan, D. R. Brigstock, A. Brisson, M. L. Broekman, J. F. Bromberg, P. Bryl-Gorecka, S. Buch, A. H. Buck, D. Burger, S. Busatto, D. Buschmann, B. Bussolati, E. I. Buzas, J. B. Byrd, G. Camussi, D. R. Carter, S. Caruso, L. W. Chamley, Y. T. Chang, C. Chen, S. Chen, L. Cheng, A. R. Chin, A. Clayton, S. P. Clerici, A. Cocks, E. Cocucci, R. J. Coffey, A. Cordeiro-da-Silva, Y. Couch, F. A. Coumans, B. Coyle, R. Crescitelli, M. F. Criado, C. D'Souza-Schorey, S. Das, A. Datta Chaudhuri, P. de Candia, E. F. De Santana, O. De Wever, H. A. Del Portillo, T. Demaret, S. Deville, A. Devitt,

B. Dhondt, D. Di Vizio, L. C. Dieterich, V. Dolo, A. P. Dominguez Rubio, M. Dominici, M. R. Dourado, T. A. Driedonks, F. V. Duarte, H. M. Duncan, R. M. Eichenberger, K. Ekstrom, S. El Andaloussi, C. Elie-Caille, U. Erdbrugger, J. M. Falcon-Perez, F. Fatima, J. E. Fish, M. Flores-Bellver, A. Forsonits, A. Frelet-Barrand, F. Fricke, G. Fuhrmann, S. Gabrielsson, A. Gamez-Valero, C. Gardiner, K. Gartner, R. Gaudin, Y. S. Gho, B. Giebel, C. Gilbert, M. Gimona, I. Giusti, D. C. Goberdhan, A. Gorgens, S. M. Gorski, D. W. Greening, J. C. Gross, A. Gualerzi, G. N. Gupta, D. Gustafson, A. Handberg, R. A. Haraszti, P. Harrison, H. Hegyesi, A. Hendrix, A. F. Hill, F. H. Hochberg, K. F. Hoffmann, B. Holder, H. Holthofer, B. Hosseinkhani, G. Hu, Y. Huang, V. Huber, S. Hunt, A. G. Ibrahim, T. Ikezu, J. M. Inal, M. Isin, A. Ivanova, H. K. Jackson, S. Jacobsen, S. M. Jay, M. Jayachandran, G. Jenster, L. Jiang, S. M. Johnson, J. C. Jones, A. Jong, T. Jovanovic-Talisman, S. Jung, R. Kalluri, S. I. Kano, S. Kaur, Y. Kawamura, E. T. Keller, D. Khamari, E. Khomyakova, A. Khvorova, P. Kierulf, K. P. Kim, T. Kislinger, M. Klingeborn, D. J. Klinke 2nd, M. Kornek, M. M. Kosanovic, A. F. Kovacs, E. M. Kramer-Albers, S. Krasemann, M. Krause, I. V. Kurochkin, G. D. Kusuma, S. Kuypers, S. Laitinen, S. M. Langevin, L. R. Languino, J. Lannigan, C. Lasser, L. C. Laurent, G. Lavieu, E. Lazaro-Ibanez, S. Le Lay, M. S. Lee, Y. X. F. Lee, D. S. Lemos, M. Lenassi, A. Leszczynska, I. T. Li, K. Liao, S. F. Libregts, E. Ligeti, R. Lim, S. K. Lim, A. Line, K. Linnemannstons, A. Llorente, C. A. Lombard, M. J. Lorenowicz, A. M. Lorincz, J. Lotvall, J. Lovett, M. C. Lowry, X. Loyer, Q. Lu, B. Lukomska, T. R. Lunavat, S. L. Maas, H. Malhi, A. Marcilla, J. Mariani, J. Mariscal, E. S. Martens-Uzunova, L. Martin-Jaular, M. C. Martinez, V. R. Martins, M. Mathieu, S. Mathivanan, M. Maugeri, L. K. McGinnis, M. J. McVey, D. G. Meckes Jr., K. L. Meehan, I. Mertens, V. R. Minciacchi, A. Moller, M. Moller Jorgensen, A. Morales-Kastresana, J. Morhayim, F. Mullier, M. Muraca, L. Musante, V. Mussack, D. C. Muth, K. H. Myburgh, T. Najrana, M. Nawaz, I. Nazarenko, P. Nejsum, C. Neri, T. Neri, R. Nieuwland, L. Nimrichter, J. P. Nolan, E. N. Nolte-'t Hoen, N. N. Hooten, L. O'Driscoll, T. O'Grady, A. O'Loghlen, T. Ochiya, M. Olivier, A. Ortiz, L. A. Ortiz, X. Osteikoetxea, O. Ostergaard, M. Ostrowski, J. Park, D. M. Pegtel, H. Peinado, F. Perut, M. W. Pfaffl, D. G. Phinney, B. C. Pieters, R. C. Pink, D. S. Pisetsky, E. P. von Strandmann, I. Polakovicova, I. K. Poon, B. H. Powell, I. Prada, L. Pulliam, P. Quesenberry, A. Radeghieri, R. L. Raffai, S. Raimondo, J. Rak, M. I. Ramirez, G. Raposo, M. S. Rayyan, N. Regev-Rudzki, F. L. Ricklefs, P. D. Robbins, D. D. Roberts, S. C. Rodrigues, E. Rohde, S. Rome, K. M. Rouschop, A. Rughetti, A. E. Russell, P. Saa, S. Sahoo, E. Salas-Huenuleo, C. Sanchez, J. A. Saugstad, M. J. Saul, R. M. Schiffelers, R. Schneider, T. H. Schoyen, A. Scott, E. Shahaj, S. Sharma, O. Shatnyeva, F. Shekari, G. V. Shelke, A. K. Shetty, K. Shiba, P. R. Siljander, A. M. Silva, A. Skowronek, O. L. Snyder 2nd, R. P. Soares, B. W. Sodar, C. Soekmadji, J. Sotillo, P. D. Stahl, W. Stoorvogel, S. L. Stott, E. F. Strasser, S. Swift, H. Tahara, M. Tewari, K. Timms, S. Tiwari, R. Tixeira, M. Tkach, W. S. Toh, R. Tomasini, A. C. Torrecilhas, J. P. Tosar, V. Toxavidis, L. Urbanelli, P. Vader, B. W. van Balkom, S. G. van der Grein, J. Van Deun, M. J. van Herwijnen, K. Van Keuren-Jensen, G. van Niel, M. E. van Royen, A. J. van Wijnen, M. H. Vasconcelos, I. J. Vechetti Jr., T. D. Veit, L. J. Vella, E. Velot, F. J. Verweij, B. Vestad, J. L. Vinas, T. Visnovitz, K. V. Vukman, J. Wahlgren, D. C. Watson, M. H. Wauben, A. Weaver, J. P. Webber, V. Weber, A. M. Wehman, D. J. Weiss, J. A. Welsh, S. Wendt, A. M. Wheelock, Z. Wiener, L. Witte, J. Wolfram, A. Xagorari, P. Xander, J. Xu, X. Yan, M. Yanez-Mo, H. Yin, Y. Yuana, V. Zappulli, J. Zarubova, V. Zekas, J. Y. Zhang, Z. Zhao, L. Zheng, A. R. Zheutlin, A. M. Zickler, P. Zimmermann, A. M. Zivkovic, D. Zocco, E. K. Zuba-Surma, Minimal information for studies of extracellular vesicles 2018 (misev2018): A position statement of the international society for extracellular vesicles and update of the misev2014 guidelines. *J. Extracell. Vesicles* **7**, 1535750 (2018).

53. D. W. Huang, B. T. Sherman, R. A. Lempicki, Systematic and integrative analysis of large gene lists using david bioinformatics resources. *Nat. Protoc.* **4**, 44 (2009).
54. S. X. Ge, E. W. Son, R. Yao, Idep: An integrated web application for differential expression and pathway analysis of rna-seq data. *BMC Bioinformatics* **19**, 534 (2018).

Acknowledgments: LC-MS was performed at the Technical University of Denmark Proteomics Core. TEM and immuno-EM of small EVs were performed at the University of Manchester Electron Microscopy Core Facility. TEM of fibroblasts was performed at the University of Copenhagen Core Facility for Integrated Microscopy. Confocal microscopy was performed at the University of Copenhagen Center for Advance Bioimaging. NTA was performed in the laboratory of J. Zhang at the Technical University of Denmark Department of Chemistry. We would like to thank M. S. Clausen and Y. Hansen (Bispebjerg Hospital Department of Clinical Biochemistry) for animal husbandry, as well as P. Zigrino (University of Cologne), K. E. Kadler and A. Pickard (University of Manchester), R. L. Miller (Copenhagen Center for Glycomics), L. H. Blicher (Technical University of Denmark Proteomics Core Facility), M. Bayer, C. Montagna, A. Giannopoulos, C. Zhang, and A. Løvind Andersen (Institute of Sports Medicine Copenhagen), V. Pless (Bispebjerg Hospital Department of Dermatology), the Bispebjerg Hospital Department of Audiology, and C. Engelbrekt (Technical University of Denmark Department of Chemistry) for the helpful discussions and providing technical support and/or access to equipment. **Funding:** This work was supported by a Lundbeck Foundation Grant (R198-2015-207 to M.K.) and a fellowship from Region Hovedstaden Bispebjerg and Frederiksberg Hospital (to C.-Y.C.Y.). J.H. is supported by the Danish Biotechnology Center for Cellular Communication. **Author contributions:** C.-Y.C.Y.: conception and design, acquisition of data, analysis and interpretation of data, and writing the manuscript. F.D.: design of analysis, analysis and interpretation of data, and reviewing the manuscript. E.M.S.: performed the LC-MS and curated the data. Y.L. and Z.Z.: acquisition of data. B.G., J.Z., J.H., and J.F.: contributed materials and analysis tools. M.K.: contributed materials and analysis tools and reviewed the manuscript. All authors approved the manuscript. **Competing interests:** The authors declare that they have no competing interests. **Data and materials availability:** The MS proteomics data have been deposited to the ProteomeXchange Consortium via the PRIDE partner repository (www.ebi.ac.uk/pride/archive/) with the dataset identifier PXD022393. All other data are available in the Supplementary Materials. All original scans of Western blots and gels are available in data file S1. Data used to generate figures and statistics can be found in data file S2.

Submitted 22 February 2021
Accepted 17 February 2022
Published 8 April 2022
10.1126/sciadv.abc9061